RSC Advances

ROYAL SOCIETY OF CHEMISTRY

www.rsc.org/advances

Journal Name

ARTICLE

Layer-by-Layer assembly modification to prepare firmly bonded Si-graphene composite for high-performance anode

Received 00th January 20xx,
Accepted 00th January 20xx

DOI: 10.1039/x0xx00000x

www.rsc.org/

Wenhui Zhang, Lin Wu, Lijuan Du, Lu Yue*, Rongfeng Guan, Qinfang Zhang*, Guihua Hou, Rong Shao

A new nanocomposite of Si nanoparticles homogenously encapsulated in graphene composite was prepared by a facile layer-by-layer (LBL) assembled modification method, followed by electrostatic attraction directed self-assembly approach and thermally reduced process. The wrinkled graphene sheets were assembled into a three-dimensional network and well covered the surface of highly dispersed Si nanoparticles. The as-prepared Si-graphene composite exhibited good electrochemical performances as an anode material in lithium-ion batteries, showing a stable reversible capacity of 1150 mAh g^{-1} with a high capacity retention rate of 92.0% over 100 cycles and high rate capability (840 mAh g^{-1} at 3000 mA g^{-1}).

Introduction

Lithium-ion battery has become the dominant rechargeable battery chemistry for consumer electronic devices and is poised to become commonplace for industrial, transportation, and power-storage applications.[1] Recently, Si materials have been considered as promising anode materials for lithium-ion batteries due to their high theoretical specific capacity of 4200 mAh g^{-1}, which is 10 times more than that of commercial graphite.[2] However, Si has major drawbacks stemming from the large volume expansion upwards of 300% during cycling and low electrical conductivity which could cause rapid capacity fading.[3, 4]

To overcome these problems, various approaches have been adopted.[5-12] Among them, surface coating for Si nanoparticles has turned out to be an economic and feasible method to improve the performance of materials by modifying the surface chemistry and providing protective layers. Recently, graphene has been extensively used and proved to be an effective surface coating layer due to its relatively low mass, good conductivity, flexibility, small volume change, and reasonable Li-insertion capacity.[13-16] Despite the improved electrochemical performance, the strategies for the synthesis of Si-based composite materials have generally focused on simple mixing and dispersing Si nanoparticles onto the surface of the graphene oxide (GO) nanosheets. The strategies do not provide good dispersion and coating of Si nanoparticles between GO sheets, leading to a limited electrochemical performance enhancement. Therefore, the uniform dispersion and effective coating of Si nanoparticles in the desired Si nanoparticle-graphene composite remains a great challenge.

The electrostatic self-assembly is a novel technique already demonstrated for preparing well-mixed nanocomposites of various sizes, shapes, and materials. The method is based on the electrostatic attraction between oppositely charged between different materials. Recently, some researchers tried to prepare Si-graphene composite using the electrostatic self-assembly by single NH_2-terminated molecules or Poly(diallyldimethylammonium chloride) (PDDA) modification. For example, Zhou et al.[17] reported a Si@NH_2/GO composite anode, which delivered a reversible capacity of 822 mAh g^{-1} after 100 cycles at 0.1 A g^{-1}. Miroshnikov et al. [18] prepared a Si-GO composite is by modification of the surface of Si with 3-aminopropyltriethoxysilane, covalent bonding to GO and further annealing to yield Si-graphene. The highly dispersed composite was found to sustain ultrafast charging and discharging. Zhou et al. [19] developed an electrostatic attraction directed self-assembly approach for fabricating a nanocomposite of Si nanoparticles encapsulated in graphene by PDDA modification. This approach realized a uniform dispersion of Si nanoparticles between two layers of graphene sheets. The as-obtained nanocomposite exhibited stable cycling performance (approximately 1205 mA h g^{-1} after 150 cycles) and excellent rate capability. Ji et al.[20] reported the use of PDDA for wrapping Si nanoparticles by GO, which displayed a reversible capacity of 370 mAh g^{-1} at 400 mA g^{-1} after 100 cycles. Tang et al. [21] developed a novel three-dimensional Si/graphene nano-porous network composite has been fabricated by steam etching Si-PDDA/graphene aerogel. The composite electrode presents high specific capacity and good cycling stability (1004 mAh g^{-1} at 50 mA g^{-1} up to100 cycles). Liu et al.[22] found that the van der Waals between the Si and GO in preparing played an important role in affecting the final composite anode performance by both experimental observations and theoretical simulations. All these

Jiangsu Collaborative Innovation Center for Ecological Building Materials and Environmental Protection Equipments / Key Laboratory for Advanced Technology in Environmental Protection of Jiangsu Province, Yancheng Institute of Technology, Jiangsu 224051, China. E-mail address: yuelu66@126.com (L. Yue), qfangzhang@gmail.com (Q. F. Zhang). Tel./fax:+ 86 0515 88298925.

work showed that the weak interactions between the heteroatoms in Si surfactants with graphene oxide act critically in enhancing the cycling stability.

The layer-by-layer (LBL) technique is a simple and versatile method to fabricate nano-structured films and can be achieved in a straight forward and low cost manner.[23, 24] A layer of polyelectrolyte, e.g. PDDA and sodium poly(styrene-sulfonate) (PSS), is first coated onto the surface in sequence of the nanostructures by LBL assembly, thus enabling the nanostructures to be positively/negatively charged. The oppositely charged ions in the solution are adsorbed onto the surface of the nanostructures due to the electrostatic attraction between the charged species.[25-27] Compared to single modification techniques (e.g. only PDDA), the LBL technique, which is based on the better electrostatic attraction between oppositely charged species, provides more versatile and powerful method to synthesize various types of hybrid nanostructures.

Herein, we report our recent work on the synthesis of new Si-graphene composite via the LBL assembly modification technique. The as-obtained electrode exhibited much improved cycling performance and good rate capability when compared with single PDDA modifiation, which provided a simple and effective strategy to design a novel Si-based electrode with good performance.

Experimental Section

Materials and Equipments

Carboxymethyl Cellulose Sodium (CMC) (Viscosity: 800-1200 mPa S) was purchased from Guangzhou Dingying Trading Co. (China). Nanosized Si powder with particle sizes of 50-200 nm was purchased from Xuzhou Jiechuang New Material Technology Co. (China). PDDA (Mw＜100,000, 35 wt% aqueous solution, 100-200 cP) was purchased from Aladdin reagent Co. (China). PSS (average MW: 70, 000) was purchased from Sigma–Aldrich Chemical Co. (USA). The electrolyte of 1M $LiPF_6$ in ethylene carbonate (EC, ≥99.9%)/diethylene carbonate (DEC, ≥99.9%)/dimethyl carbonate (DMC, ≥99.9%) (v/v/v=1/1/1) was purchased from Zhangjiagang Guotai-Huarong New Chemical Materials Co. (China) (water content <10 ppm). Other reagents used in this work were purchased from Sinopharm Group Pharmaceutical Co. (China). GO nanosheets were prepared from natural graphite using a modified Hummers 'method. All the reagents were used without further purification.

The morphology of the samples was observed by a scanning electron microscope (SEM; Hitachi S-4800, Japan) and transmission electron microscope (TEM; JEOL JEM 2100F, Japan). The phase identification was performed by X-ray diffraction (XRD, Siemens D5005) from 5° to 80°. Attenuated total reflection Fourier-transform infrared (ATR-FTIR) spectroscopy was recorded on a Nicolet Magna 550 spectrometer from 4000 to 670 cm^{-1} at resolution of 4 cm^{-1}. The XPS spectra were obtained with ESCALAB250 XPS (Thermo Fisher Scientific, USA). Electrochemical impedance spectroscopy (EIS) results were obtained with Zennium/IM6 electrochemical workstation (Zahner, Germany).

Preparation of Si-graphene composite

Fig. 1 shows the fabrication process of Si-graphene composite by LBL assembly modification. Firstly, nanosized Si powder was calcined in ambient air at 600 °C for 1 h to form a layer of SiO_2 coating on the surface (named as $Si@SiO_2$). For LBL technique, the $Si@SiO_2$ was immersed into PDDA-PSS-PDDA solution in turn. This procedure produced a positively charged sandwich layer of PDDA and PSS on the final surface of $Si@SiO_2$. Subsequently, the modificated $Si@SiO_2$ was compactly attracted by GO in solution. The final Si-graphene composite was obtained by thermo-reduction process. A typical procedure was described as follows. 1.0 g $Si@SiO_2$ was sonicated for 1 h in 200 mL of 0.2 M NaCl solution, and the 2.057 g PDDA (3.6 mg/mL) was added. The above-mentioned solution was sonicated for 1 h and stirred for another 6 h. Then, the excess PDDA was removed by centrifugation. The PDDA-modified $Si@SiO_2$ was sonicated for 1 h in 200 mL of 3.6 mg/mL PSS solution and stirred for another 6 h. Subsequently, the PDDA/PSS-modified $Si@SiO_2$ was dispersed in 3.6 mg/mL PDDA contained 0.2 M NaCl solution by sonicating and stirring again. The final PDDA/PSS/PDDA-modified $Si@SiO_2$ was collected, washed with distilled water for several times and then dried in air at 60 °C over night. 0.1 g PDDA/PSS/PDDA-modified $Si@SiO_2$ was dispersed in 200 mL deionized water under ultrasonication for 1 h. The suspension of PDDA/PSS/PDDA-modified $Si@SiO_2$ in water was added dropwise into 200 mL GO aqueous dispersion (~0.15 mg mL^{-1}, pH 6.0) under fast stirring (400 rpm) for 2 h. The precipitate was filtered and washed by ethanol three times, followed by a thermal treatment at 800 °C in a furnace for 3 h under an Ar atmosphere (The sample referred as Si-LBL/G composite). For comparison, the unmodificated and PDDA-modificated $Si@SiO_2$ composed with GO were also prepared in a similar process, named as Si/G and Si-PDDA/G composite. The carbon content in Si-graphene composite was determined to be 23.4 wt.% using thermogravimetric analysis.

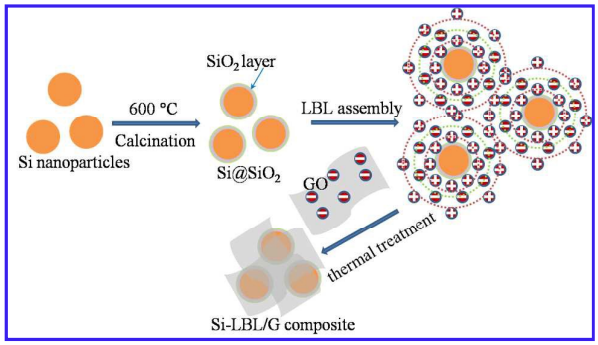

Fig. 1 Schematic of the fabrication of Si-LBL/G composite.

Characterization of electrochemical performance

The coin cells (CR2025) were assembled to test the electrochemical performances of the as-prepared electrodes. The as-prepared samples were mixed with acetylene black and carboxymethyl cellulose, in a weight ratio of 60:20:20 in an aqueous solution to form homogeneous slurry. The slurry was spread onto a 10 μm thick copper foil and dried at 60 °C for 12 h in a vacuum oven and then pressed to obtain the electrode sheet with a 9-10 μm coating thickness and a loading level of about 1.4 mg cm-2. The cells were assembled in an Ar filled glove-box, using 1 M $LiPF_6$ EC/DEC/DMC (1:1:1 by volume) as the electrolyte. The cells were

charged and discharged galvanostatically in the fixed voltage window from 10 mV to 1.5 V on a Shenzhen Neware battery cycler (China) at 25 °C. All the gravimetric capacity data related to as-prepared samples were based on the mass of both Si and carbon. EIS was measured by applying an alternating voltage of 5 mV over the frequency ranging from 10^{-2} to 10^{5} Hz.

Results and Discussion

The new Si-graphene composite was fabricated by a facile LBL technique by modifying the Si nanoparticles through PDDA/PSS/PDDA solution in turn before mixing with GO and followed by thermal reduction process. Fig. 2 presents the XRD patterns of Si@SiO_2, GO, reduced GO (rGO), Si-LBL/G, Si-PDDA/G and Si/G. Si@SiO_2 presented typical diffraction peaks at 2θ of about 28.4°, 47.4°, 56.2°, 69.2° and 76.5°, corresponding to the (111), (220), (311), (400) and (331) plane of Si, respectively.[28] The diffraction peak around 26.4° for graphite has been not found in the GO pattern, and a broad peak has arisen at 2θ=10.9°, indicating the successful oxidation of raw graphite to graphite oxide. For the thermally rGO, the broad diffraction peaks at about 2θ=25.0° can be attributed to graphite-like (002) structure.[29, 30] After carbonization process, the diffraction of Si for the sample of Si-LBL/G, Si-PDDA/G and Si/G showed not change, indicating that the pyrolysis did not destroy the original Si crystalline structure, whereas the graphite diffraction peaks were absent.

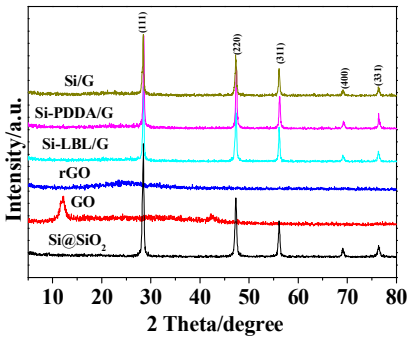

Fig. 2 XRD patterns for Si@SiO2, GO, rGO, Si-LBL/G, Si-PDDA/G and Si/G.

Fig. 3 showed the ATR-FTIR spectra of these samples. For PDDA sample, a strong peak at ~3440 cm^{-1} in Fig. 3a was attributed mainly to -NR_3^+ stretching vibration, the peaks around the 3000-2800 cm^{-1} region and 1460 cm^{-1} were assigned to the C-H bending, the peak at 1614 cm^{-1} in FTIR spectrum for PDDA was attributed to the deformation vibration of –NH, the absorption peak at 1253 cm^{-1} was attributed to C-N stretching vibration.[31-35] The spectrum of PSS mainly showed peaks at 1125 cm^{-1} and 1038 cm^{-1}, which could be assigned to the symmetric and asymmetric stretching vibrations of the sulfonate groups, respectively.[36] For Si sample, only a Si-O-Si stretching vibration peaks at 1240 cm^{-1} could be observed in the spectrum. The spectrum of Si@SiO_2 mainly showed the Si-O-Si bending vibrations at 820 cm^{-1}, the stretching vibrations at 1060 and 1240 cm^{-1} and the O-H stretching vibration at ~3480 cm^{-1}[37]. For the Si@SiO_2-PDDA sample, except the characteristic absorption band of Si-O-Si, a bending peak of C-H at 1464 cm^{-1}, a deformation vibration peak of –NH and a stretching vibration of -NR_3^+ at ~3380 cm^{-1} also could be observed in the spectra clearly, implying the presence of PDDA in the surface of Si@SiO_2. It is worth noting that the C-H bending around the 3000-2800 cm^{-1} region attributed to the PDDA also could be observed in the spectrum for Si@SiO_2-PDDA:PSS:PDDA sample, which was powerful evidence that there were more adsorption for PDDA on Si@SiO_2. What's more, a weak at 1038 cm^{-1} attributed to PSS could be observed in the spectra. These results suggested the formation of strong bond and adsorption between the hydroxylated Si surface and polyelectrolyte (PDDA and PSS) after Si@SiO_2 being modificated by LBL method. As shown in Figure 3b, the most characteristic features of GO included the broad, intense band of O-H stretching vibration at 3000-3700 cm^{-1}, as well as the bands of carbonyl, carboxyl and epoxy functional groups stretching vibration at 1740 cm^{-1}, 1600 cm^{-1} and 1050 cm^{-1}, respectively, demonstrating that the GO had abundant oxygen containing groups.[38-40] For the spectra of rGO and Si-graphene nanocomposites (Si/G, Si-PDDA/G and Si-LBL/G) in Figure 3b, the strong absorption at 1060 and 1140 cm^{-1} was attributed to the stretching vibrations and the antisymmetrical vibration of Si-O-Si. Besides, compared to GO, the intensities of the bands corresponding to the oxygen functional groups and O-H stretching vibration in these composite obviously decreased, suggesting the effective reduction of GO sheets by thermal treatment.

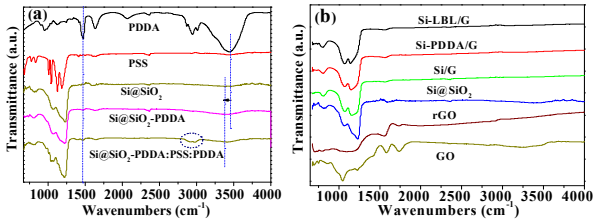

Fig. 3 (a) ATR-FTIR spectra of Si@SiO_2, PDDA-modified Si@SiO_2, PDDA/PSS/PDDA-modified Si@SiO_2, PDDA and PSS; (b) ATR-FTIR spectra of Si@SiO_2, raw Si, GO, rGO, Si-LBL/G, Si-PDDA/G and Si /G.

XPS measurements provided further evidence of the strong bonding between PDDA or/and PSS and Si nanoparticles [41]. As shown in Fig. 4, the existence of C (C1s, 284.3 eV), O (O1s, 531.8eV), S (S2s, 168.99eV) and Na (Na2s, 63.4eV; Na1s, 1072.6eV) in PSS was evident. For PDDA, except existence of C and O, there was an N1s peak at the binding energy of 400.3 eV in the XPS survey spectra. For Si@SiO_2, the existence of Si (Si2p, 106.0 eV; Si2s, 158.0), O (O1s, 531.8eV) was evident. When compared with PDDA-modified Si@SiO_2, PDDA/PSS/PDDA-modified Si@SiO_2 and Si@SiO_2, we can find that there were strong signals for C and N peaks. What's more, the peaks for S and Na could also be clearly observed in the PDDA/PSS/PDDA-modified Si@SiO_2 spectra. According to the XPS tests, it can be obtained that the atomic ratio of C was about 1.4:1 for PDDA/PSS/PDDA-modified and PDDA-modified Si@SiO_2. All these results implied that more PDDA and some PSS were bound to the hydroxylated Si surface and involved in the adsorption process for PDDA/PSS/PDDA-modified Si@SiO_2, which was in good agreement with the ATR-FTIR analysis.

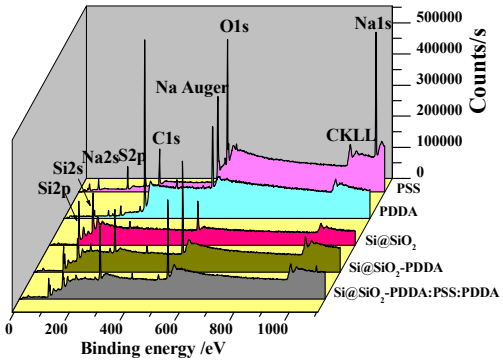

Fig. 4 XPS of $Si@SiO_2$, PDDA-modified $Si@SiO_2$, PDDA/PSS/PDDA-modified $Si@SiO_2$, PDDA and PSS.

From Fig. 5a/b, it can be first observed that both $Si@SiO_2$ nanoparticles and GO showed good dispersion to water. Due to the lack of electrostatic attraction, when the unmodificated $Si@SiO_2$ nanoparticles were mixed with GO solution, there were no bonds between the GO and $Si@SiO_2$. As a result, Si could not form a homogeneous composite with GO (Si nanoparticles precipitated after the suspension standing for one day, but GO still remained suspended in solution in Fig. 5c). When compared with unmodificated $Si@SiO_2$, the PDDA-modificated $Si@SiO_2$ and PDDA:PSS:PDDA-modificated $Si@SiO_2$ could render the Si nanoparticle's surface to be positively charged in the solution due to the ionization of amino groups. After diluting the modificated $Si@SiO_2$ suspension into the GO suspension and mild magnetic stirring for 24 h, the precipitates formed to leave a transparent aqueous solution (Fig. 5d/e), indicating that hybrid assembled between positively charged Si nanoparticles and negatively charged GO by electrostatic interactions occurred to form Si-graphene composites.

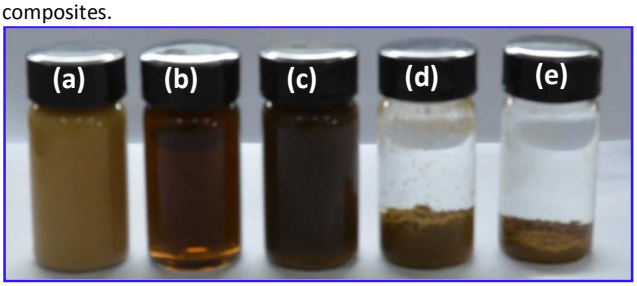

Fig. 5 The photos of (a) $Si@SiO_2$ suspension, (b) GO suspension, (c) Si/G suspension, (d) Si-PDDA/G precipitate and (e) the resulting Si-LBL/G precipitate.

After thermal reduction of the Si-graphene composites at 800 °C for 3 h under Ar, the Si-graphene composites were obtained. Fig. 6a/b show TEM images of Si/G sample after thermal treatment. These images clearly confirmed the existence of transparent and rippled GO sheets or stacked multilayer GO sheets. Si nanoparticles with a particle size of 50–200 nm were dispersed on the surface of the GO sheets. However, there were almost no Si nanoparticles wrapped in the GO shell. The Si nanoparticles were separated from each other and there were large spaces among the nanoparticles. In this case, GO could not form an effective coating layer on the Si surface. Fig. 6c/d show TEM images of Si-PDDA/G sample after thermal treatment. These images clearly confirmed large sized aggregates were formed, and the space between Si particles and GO became small. When compared with Si-PDDA/G sample, Si-LBL/G displayed micrometre-sized aggregates, and the space between Si nanoparticles and GO became smaller in Fig. 6e. The higher magnified TEM image (Fig. 6f-h) shows that the Si nanoparticles were well embedded and uniformly dispersed into the crumpled, flexible GO sheets. The presence of wrinkles and folds was the characteristic feature of GO sheets. No any obvious aggregation of Si nanoparticles could be found, and the typically wrinkled GO sheets formed a network and covered the highly dispersed Si nanoparticle well.

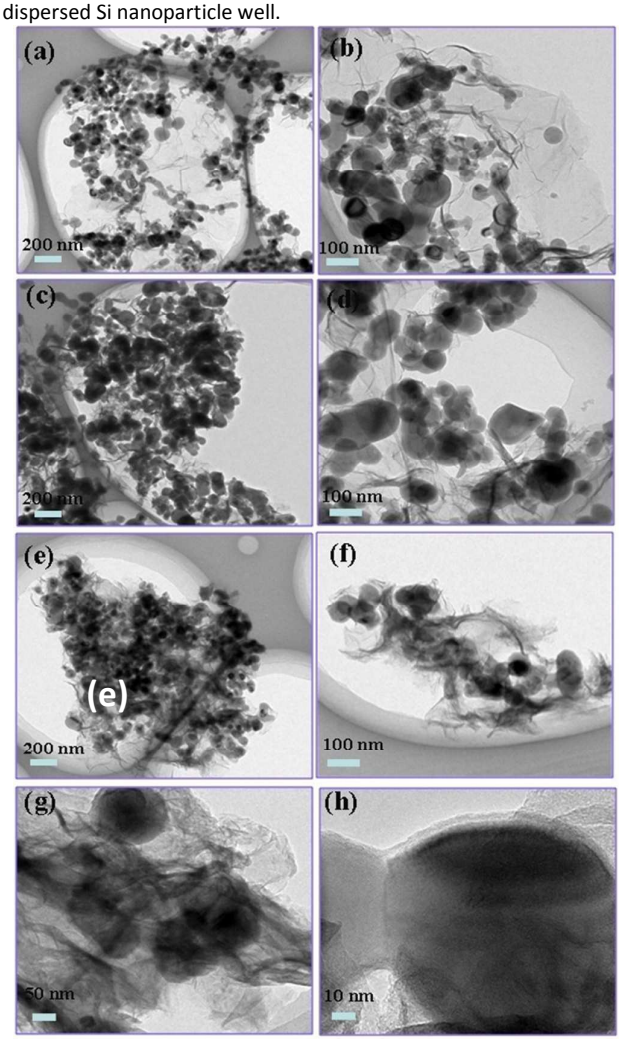

Fig. 6 TEM images of (a/b) Si/G, (c/d) Si-PDDA/G and (e-h) Si-LBL/G composite.

The CV measurement (Fig. 7a) was carried out to investigate the electrode reaction at a scan rate of 0. 5 mV s^{-1}. The reduction and oxidation peaks of rGO electrode appeared around 0.31 and 0.27 V versus Li^+/Li correspond to the insertion and extraction of

lithium ions into/from GO layers, respectively.[38] The first discharge process (negative scan) of the Si-LBL/G electrode showed a broad peak around 1.2-1.0 V and a sharp reduction peak below 0.3 V, corresponding to the formation of SEI film and the insertion of Li^+ into Si, respectively.[13] In the subsequent charge process (positive scan), two broad oxidation peaks appeared at 0.38 and 0.52 V which could be attributed to the partial decomposition of the Li_xSi and the extraction of Li^+ from the Si host, respectively.[42] Besides, when compared with rGO electrode, the Si-LBL/G electrode displayed a higher peak current, indicating a higher lithiation/delithiation capacity.

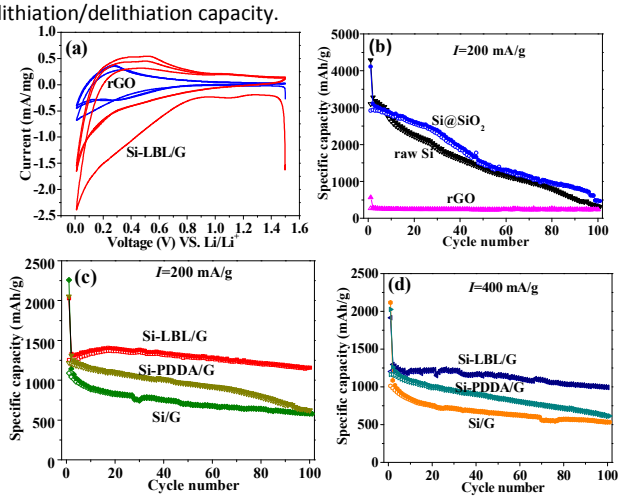

Fig. 7 (a) Cyclic voltammograms of rGO and Si-LBL/G composite electrode in the voltage range of 0.01–1.5 V at a scan rate 0.5 mV s^{-1}; (b) Cycling stability of raw Si, $Si@SiO_2$ and rGO at 200 mA g^{-1}; (c/d) Cycling stability of Si/G, Si-PDDA/G and Si-LBL/G electrodes at a rate of 200 mA g^{-1} and 400 mA g^{-1}.

The cycling performances of raw Si, $Si@SiO_2$ and rGO electrode at a current density of 200 mA g^{-1} were displayed in Fig. 7b. The rGO electrode showed an initial discharge capacity of 570 mAh g^{-1} which was about 1.5 times higher than the graphite electrode. But, the rGO electrode could only retain a reversible discharge capacity of 240 mAh g^{-1} after 100 cycles and a low initial coulomb efficiency of 47%. The $Si@SiO_2$ electrode showed a slightly lower initial discharge/charge capacity of 4113/2919 mAh g^{-1} compared with that of the raw Si electrode (4295/3100 mAh g^{-1}), but had better cycling performance. It was known that the SiO_2 on the surface of Si might not only sacrifice some lithium storage capacity, but also act as a protective layer to prevent the volume expansion to some extent. When compared with the cycling performance of GO and Si electrode, one owned the good cyclical stability but low capacity, the other had a higher lithiation/delithiation capacity but poor stability, it was necessary for us to find a compromise and reasonable approach to prepare a composite material of them.

The cycling performances of Si/G, Si-PDDA/G and Si-LBL/G electrode at a current density of 200 mA g^{-1} and 400 mA g^{-1} were displayed in Fig. 7c/d. At 200 mA g^{-1}, the Si/G electrode delivered a high initial charge/discharge capacity of 1089/2259 mAh g^{-1} with coulombic efficiency of 48.2%, and exhibited a high charge/discharge capacity of 577/581 mAh g^{-1} over 100 cycles. Compared with $Si@SiO_2$, Si/G electrode delivered higher charge capacity retention rate of 52%. It was known that the GO on the surface of Si materials might sacrifice some lithium storage capacity, but also act as a protective layer to prevent the volume expansion and improve the electronic conductivity. Si-PDDA/G and Si-LBL/G electrode delivered an initial charge/discharge capacity of 1219/2053 mAh g^{-1} with coulombic efficiency of 59.3%, and 1257/2029 mAh g^{-1} with a coulombic efficiency of 61.9%, respectively. The charge capacity retention rate of the Si-PDDA/G and Si-LBL/G electrode was 50.8 and 92.0% over 100 cycles, respectively. At 400 mA g^{-1}, the electrodes showed similar results. No doubt, the Si-LBL/G electrode displayed an outstanding cycling stability.

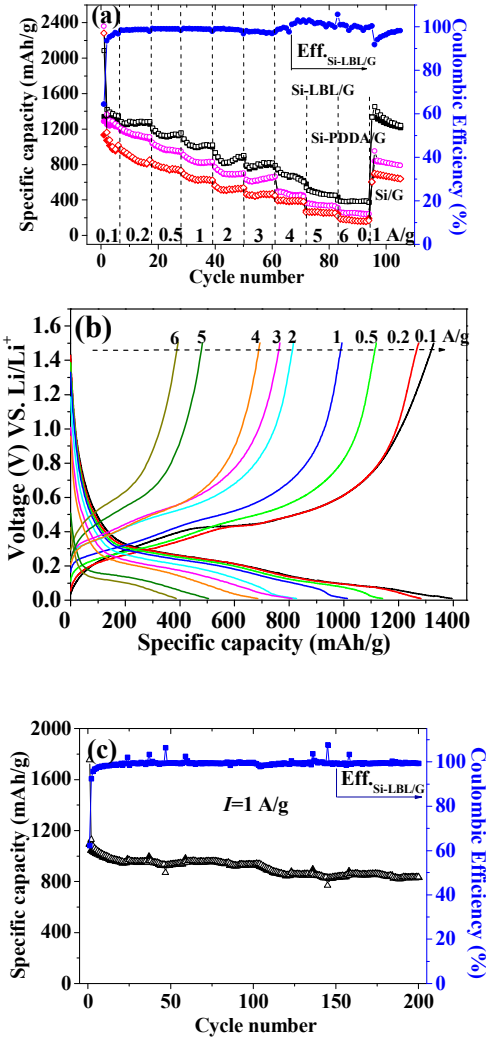

Fig. 8 (a) Rate performance of Si/G, Si-PDDA/G and Si-LBL/G electrodes; (b) voltage profiles of Si-LBL/G electrode during the rate capability test; (c) Long-term cycling performance of Si-LBL/G electrode at a rate of 1 A g^{-1}.

Due to the improved cycling stability of the Si-graphene composite electrodes, we also tested their rate capability (Fig. 8). The electrodes were cycled at a current density of 100 mA g^{-1} for

the initial 6 cycles. Then the current density was increased gradually to 6 A g^{-1} and finally returned to 100 mA g^{-1} again. The Si/G electrode showed a first charge/discharge capacity of 1134/2280 mAh g^{-1} with a coulombic efficiency of 49.7%. After 6 cycles, the coulombic efficiency was increased to 99%. At higher current density of 0.2, 0.5, 1, 2, 3, 4, 5 and 6 A g^{-1}, the capacity of Si/G electrode drops to about 876, 761, 639, 517, 465, 402, 273 and 167 mAh g^{-1}, respectively. When reducing the current density back to 100 mA g^{-1}, the reversible capacity was only raised to 604 mAh g^{-1}. When compared with Si/G electrode, Si-PDDA/G displayed a better rate performance, which showed an average reversible capacity of 1130, 989, 823, 692, 630, 482, 360 and 264 mAh g^{-1} at the high current density, respectively. For the Si-LBL/G electrode, at the high current density, the electrode showed a metastable average reversible capacity of 1295, 1146, 1033, 876, 840, 692, 491 and 404 mAh g^{-1}, respectively. When reducing the current density back to 100 mA g^{-1}, the reversible capacity was quickly raised to 1335 mAh g^{-1}. The long-term cycling performance of Si-LBL/G electrode at a rate of 1 A g^{-1} are shown in Fig. 8c, which exhibited reversible discharge capacity of 836 mAh g^{-1} with a fading rate of 0.13%/cycle over 200 cycles. The excellent cycling performance and rate capability of Si-LBL/G nanocomposite could be ascribed to the following: i) the wrinkled and fold GO sheets formed a network and covered the highly dispersed Si nanoparticle well. The homogenous and effective GO protective layer on Si nanoparticles could deliver sufficient electrons to the Si nanoparticles, buffer the deformation pressure from Li-Si alloy and dealloy process, and preserve an integrity of the overall electrode; ii) the existence of nanospaces between wrinkled GO sheets and Si nanoparticles could enhance Li^+ diffusion to the encapsulated Si nanoparticles, as well as accommodate the volume changes of Si nanoparticles. Fig. 9 shows the TEM images of Si-LBL/G composite electrode after 100 cycles, it can found that Si nanoparticles were still well dispersed into the crumpled, flexible GO sheets after repeated Li charge/discharge process.

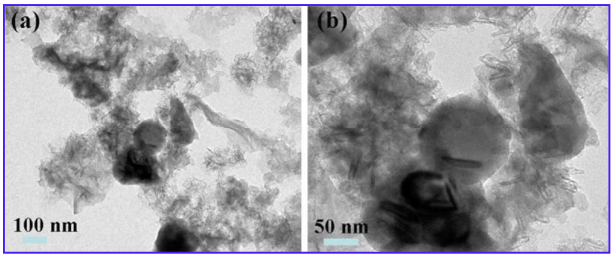

Fig. 9 TEM images of Si-LBL/G composite electrode after cycling.

To investigate the difference of electrochemical performance, EIS was employed to characterize the impedance properties of Si/G, Si-PDDA/G and Si-LBL/G electrodes. The Nyquist complex plane impedance plots of the electrodes after different charge–discharge cyclic process were presented in Fig. 10. Based on the behavior of these EIS spectra and the aforementioned studies, a suggested equivalent circuit for the Nyquist plots of these electrodes was shown in Fig. 11a.[43] This equivalent circuit was consisted of a series of four resistors elements, three constant phase elements (*CPE*) and a Warburg diffusion element. In the equivalent circuit, R_1 was composed of the electrolyte resistance (*R*s) and the electrode resistance (*R*e); R_2 represented the solid electrolyte interface (SEI) film resistances; R_3 was the interphase electronic contacts resistance; R_4 represented the charge-transfer resistance across electrode/electrolyte interface; CPE_1 and CPE_2 was attributed by the Li-ion diffusion in the SEI film and pore channel of the electrode materials, respectively; CPE_3 was the electric double-layer capacitance of electrode/solution interface; the Z_W represented Warburg impedance was related to the semi-infinite diffusion of lithium ions into the bulk electrode.[44]

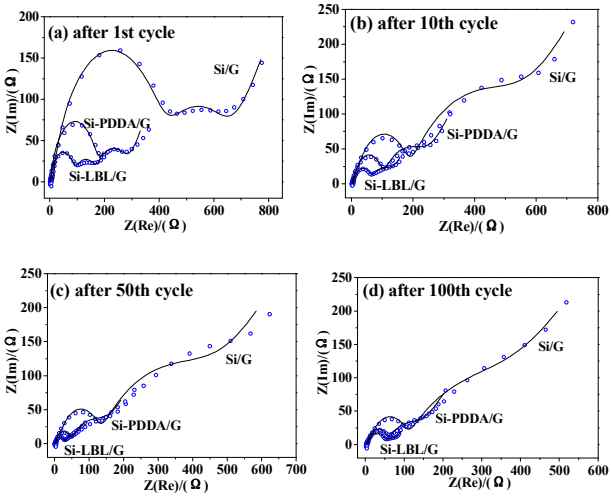

Fig. 10 Nyquist plots for Si/G, Si-PDDA/G and Si-LBL/G electrodes after 1 (a), 10 (b), 50 (c) and 100 (d) cycles; the spots correspond to the experimental data, the solid lines stand for the calculated data from the equivalent circuits in Fig. 10a.

The fitted impedances (solid lines in Fig. 10) using the equivalent circuit agreed well with the actual impedance data. By fitting the impedance data, the typical parameters were obtained and summarized in Fig. 11b-d. It was seen that the resistance change of R_1, R_2, R_3 and R_4 was smaller for both Si-PDDA/G and Si-LBL/G electrodes during cycling in Fig. 11b. Si-PDDA/G and Si-LBL/G electrodes had smaller R_1 value than Si/G during cycling, which meant that the electronic conductivity was improved when the Si nanoparticles were modified by PDDA and LBL methods before composing with GO. The smallest of R_2 in Si-LBL/G composite was observed. That is because that a stable SEI film was formed after GO coating using LBL methods, which decreased the resistance for Li^+ migration through the surface film. In addition, the smaller R_3 was also observed in Si-LBL/G composite, which usually favored the fast transport of Li^+ ions and the electrons across the interface. It also indicates that the carbon layer supplied fast charge-transfer channels on the interface of Si and electrolyte. The capacity variation of different electrodes during cycling was given in Fig. 11c. It can be seen that the $Y_{0,1}$, $Y_{0,2}$ and $Y_{0,3}$ of the Si-LBL/G composite electrode were higher than Si/G and Si-PDDA/G electrodes. The increase of $Y_{0,3}$ representing the electric double-layer capacitance favored the charge transfer for the electrode reaction. And the increase of $Y_{0,1}$ and $Y_{0,2}$ favored the diffusion of Li^+ in the SEI film and within the pore channels of wrinkled GO sheets in the

electrode, respectively. When compared with Warburg impedance for different electrodes in Fig. 11d, it can be found that there was the smallest Z_W value for Si/G electrode during cycling, which was related to the favorable diffusion of Li^+ into the bulk electrode.

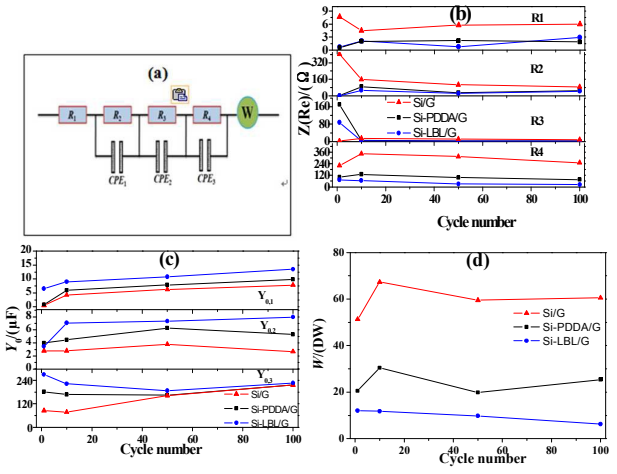

Fig. 11 (a) Equivalent circuit used to model the impedance spectra in Fig. 9; (b) Variation of resistance (b), capacity (c) and diffusion (d) for Si/G, Si-PDDA/G and Si-LBL/G electrodes during the cycles calculated from fitting the Nyquist plots in Fig. 9, respectively.

For the Si-LBL/G electrode, which owns the least value of R_4 during cycling, corresponding to the charge-transfer resistance in the electrode/electrolyte interface, was about one-third and one-tenth of that for the Si/G and Si-PDDA/G electrodes after 100 cycles. This can be explained why the Si-LBL/G electrode still owned the high capacity retention when undergo repeated lithiation/delithiation process. The homogenous and effective GO protective layer on Si nanoparticles could suppress the huge volume changes and protect the structure integrity. Based on the above EIS analysis, Si-LBL/G electrode exhibited favorable kinetic behavior, the lowest resistance and the highest capacitance, thus best cycling and rate performance among the Si-graphene composite electrodes.

Conclusions

The new Si-graphene composite was fabricated by a facile LBL assembly modification followed by thermal reducton. The typically wrinkled GO sheets formed a network and cover the highly dispersed Si nanoparticle well. The existence of nanospaces between wrinkled GO sheets and Si nanoparticles could enhance Li^+ diffusion to the encapsulated Si nanoparticles, as well as accommodate the volume changes of Si nanoparticles. The as-obtained Si-graphene composite structure exhibited excellent cycling performance and rate capability as an anode, showing a high capacity retention rate of 92.0% over 100 cycles, which made it a simple and effective strategy to design a novel Si-based electrode with good performance. In addition to Si, this simple and effective strategy can also be applied to other high capacity alloy-type anode composite materials for next generation lithium-ion batteries to improve cycle life and rate performance.

Acknowledgements

This study is supported by the National Natural Science Foundation of China (No. 51402252), the Natural Science Foundation of Jiangsu Province (No. BK20140463), China Spark Program (No. 2014GA690165), Qing Lan Project and Jiangsu Collaborative Innovation Center for Ecological Building Materials and Environmental Protection Equipments.

Notes and references

1. I. Kovalenko, B. Zdyrko, A. Magasinski, B. Hertzberg, Z. Milicev, R. Burtovyy, I. Luzinov and G. Yushin, *Science*, 2011, **334**, 75-79.
2. M. N. Obrovac and V. L. Chevrier, *Chem. Rev.*, 2014, **114**, 11444-11502.
3. D. Larcher and J. M. Tarascon, *Nat. Chem.*, 2015, **7**, 19-29.
4. J. R. Szczech and S. Jin, *Energ. Environ. Sci.*, 2011, **4**, 56-72.
5. J. B. Goodenough and K. S. Park, *J. Am. Chem. Soc.*, 2013, **135**, 1167-1176.
6. X. Su, Q. L. Wu, J. C. Li, X. C. Xiao, A. Lott, W. Q. Lu, B. W. Sheldon and J. Wu, *Adv. Energy Mater.*, 2014, **4**, 1-23.
7. M. L. Terranova, S. Orlanducci, E. Tamburri, V. Guglielmotti and M. Rossi, *J. Power Sources*, 2014, **246**, 167-177.
8. Z. L. Zhang, Y. H. Wang, Q. Q. Tan, D. Li, Y. F. Chen, Z. Y. Zhong and F. B. Su, *Nanoscale*, 2014, **6**, 371-377.
9. L. Yue, S. Q. Wang, X. Y. Zhao and L. Z. Zhang, *J. Mater. Chem.*, 2012, **22**, 1094-1099.
10. C. L. Pang, H. W. Song, N. Li and C. X. Wang, *Rsc Adv.*, 2015, **5**, 6782-6789.
11. H. H. Li, J. W. Wang, X. L. Wu, H. Z. Sun, F. M. Yang, K. Wang, L. L. Zhang, C. Y. Fan and J. P. Zhang, *Rsc Adv.*, 2014, **4**, 36218-36225.
12. Y. F. Chen, N. Du, H. Zhang and D. R. Yang, *Rsc Adv.*, 2015, **5**, 46173-46180.
13. D. Shao, D. P. Tang, Y. J. Mai and L. Z. Zhang, *J. Mater. Chem. A*, 2013, **1**, 15068-15075.
14. J. Park, G. P. Kim, I. Nam, S. Park and J. Yi, *Nanotechnology*, 2013, **24**, 025602.
15. L. Yue, W. H. Zhang, J. F. Yang and L. Z. Zhang, *Electrochim. Acta*, 2014, **125**, 206-217.
16. L. Yue, H. X. Zhong, D. P. Tang and L. Z. Zhang, *J. Solid State Electr.*, 2013, **17**, 961-968.
17. M. Zhou, F. Pu, Z. Wang, T. W. Cai, H. Chen, H. Y. Zhang and S. Y. Guan, *Phys. Chem. Chem. Phys.*, 2013, **15**, 11394-11401.
18. Y. Miroshnikov, G. Grinbom, G. Gershinsky, G. D. Nessim and D. Zitoun, *Faraday. Discuss.*, 2014, **173**, 391-402.
19. H. Tang, J. Zhang, Y. J. Zhang, Q. Q. Xiong, Y. Y. Tong, Y. Li, X. L. Wang, C. D. Gu and J. P. Tu, *J. Power Sources*, 2015, **286**, 431-437.
20. J. Y. Ji, H. X. Ji, L. L. Zhang, X. Zhao, X. Bai, X. B. Fan, F. B. Zhang and R. S. Ruoff, *Adv. Mater.*, 2013, **25**, 4673-4677.
21. X. S. Zhou, Y. X. Yin, L. J. Wan and Y. G. Guo, *Adv. Energy Mater.*, 2012, **2**, 1086-1090.

22. X. Liu, Y. C. Du, L. Y. Hu, X. S. Zhou, Y. F. Li, Z. H. Dai and J. C. Bao, *J. Phys. Chem. C*, 2015, **119**, 5848-5854.
23. R. M. Iost and F. N. Crespilho, *Biosens. Bioelectron.*, 2012, **31**, 1-10.
24. N. Du, H. Zhang, P. Wu, J. X. Yu and D. R. Yang, *J. Phys. Chem. C*, 2009, **113**, 17387-17391.
25. H. Ai, M. Fang, S. A. Jones and L. Y. M., *Biomacromolecules*, 2002, **3**, 560-564.
26. P. Wu, H. Wang, Y. W. Tang, Y. M. Zhou and T. H. Lu, *Acs Appl. Mater. Inter.*, 2014, **6**, 3546-3552.
27. N. Du, H. Zhang, B. D. Chen, X. Y. Ma, Z. H. Liu, J. B. Wu and D. R. Yang, *Adv. Mater.*, 2007, **19**, 1641-1645.
28. S. H. Ng, J. Wang, D. Wexler, S. Y. Chew and H. K. Liu, *J. Phy. Chem. C*, 2007, **111**, 11131.
29. S. H. Park, H. K. Kim, D. J. Ahn, S. I. Lee, K. C. Roh and K. B. Kim, *Electrochem. Commun.*, 2013, **34**, 117-120.
30. L. Gan, H. J. Guo, Z. X. Wang, X. H. Li, W. J. Peng, J. X. Wang, S. L. Huang and M. R. Su, *Electrochim. Acta*, 2013, **104**, 117-123.
31. Z. X. Xu, C. Y. Hu and G. X. Hu, *Thin Solid Films*, 2011, **519**, 4324-4328.
32. S. S. Ugur, M. Sariisik and H. Aktas, *Fiber. Polym.*, 2011, **12**, 190-196.
33. D. Lee and T. H. Cui, *Ieee Sens. J.*, 2009, **9**, 449-456.
34. X. Yang, S. Johnson, J. Shi, T. Holesinger and B. Swanson, *Sensor. Actuat. B-Chem*, 1997, **45**, 87-92.
35. H. J. Chen, Y. L. Wang, Y. Z. Wang, S. J. Dong and E. K. Wang, *Polymer*, 2006, **47**, 763-766.
36. C. M. Li, J. Yang, P. Y. Wang, J. Liu and Q. H. Yang, *Micropor. Mesopor. Mat*, 2009, **123**, 228-233.
37. K. Chen, Z. H. Bao, D. Liu, X. R. Zhu, Z. H. Zhang and B. Zhou, *Acta Phys-chim. Sin.*, 2011, **27**, 2719-2725.
38. P. C. Lian, X. F. Zhu, S. Z. Liang, Z. Li, W. S. Yang and H. H. Wang, *Electrochim. Acta*, 2010, **55**, 3909-3914.
39. D. F. Wang, F. L. Li, G. X. Ping, D. Chen, M. Q. Fan, L. S. Qin, L. Q. Bai, G. L. Tian, C. J. Lu and K. Y. Shu, *Int. J. Electrochem. Sc.*, 2013, **8**, 9618-9628.
40. J. Y. Zhu, L. G. Xu and J. H. He, *Chem-eur. J.*, 2012, **18**, 16393-16401.
41. L. Yue, L. Z. Zhang and H. X. Zhong, *J. Power Sources*, 2014, **247**, 327-331.
42. H. Tang, J. P. Tu, X. Y. Liu, Y. J. Zhang, S. Huang, W. Z. Li, X. L. Wang and C. D. Gu, *J. Mater. Chem. A*, 2014, **2**, 5834-5840.
43. W. H. Zhang, L. Yue, F. Zhang, Q. F. Zhang, X. C. Gui, R. F. Guan, G. H. Hou and N. Xu, *J. Mater. Chem. A*, 2015, **3**, 6102-6109.
44. L. Yue, W. H. Zhang, W. D. Zhang, Q. F. Zhang, R. F. Guan, G. H. Hou and N. Xu, *Electrochim. Acta*, 2015, **160**, 123-130.

Layer-by-Layer assembly modification to prepare firmly bonded Si-graphene composite for high-performance anode

Wenhui Zhang, Lin Wu, Lijuan Du, Lu Yue*, Rongfeng Guan, Qinfang Zhang*, Guihua Hou, Rong Shao

Jiangsu Collaborative Innovation Center for Ecological Building Materials and Environmental Protection Equipments / Key Laboratory for Advanced Technology in Environmental Protection of Jiangsu Province, Yancheng Institute of Technology, Jiangsu 224051, China

Graphical abstract: The new Si-graphene composite was fabricated by a facile LBL technique followed by thermal reduction, which exhibited excellent cycling performance and rate capability as an anode, showing a high capacity retention rate of 92.0% over 100 cycles.